

Reverse Monte Carlo analysis of the local order in liquid $\text{Ge}_{0.15}\text{Te}_{0.85}$ alloys combining neutron scattering and x-ray absorption spectroscopy

Marie-Vanessa Coulet

Laboratoire TECSEN, UMR 6122, CNRS-Université Paul Cézanne, Campus de St Jérôme, 13397 Marseille Cedex 20, France

Denis Testemale

SNBL/ESRF, 6 rue Jules Horowitz, Boîte Postale 220, 38043, Grenoble, France

Jean-Louis Hazemann

*Laboratoire de Cristallographie, 25 Avenue des Martyrs, Boîte Postale 166, 38043 Grenoble, France
and European Synchrotron Radiation Facility, 6 rue Jules Horowitz, Boîte Postale 220, 38043 Grenoble, France*

Jean-Pierre Gaspard

Physique de la Matière Condensée, B5, Université de Liège, B4000 Sart-Tilman, Belgium

Christophe Bichara

Centre de Recherches en Matière Condensée et Nanosciences-CNRS, Campus de Luminy, Case 913, F13288 Marseille, France

(Received 6 July 2005; revised manuscript received 6 September 2005; published 28 November 2005)

The structure of liquid $\text{Ge}_{0.15}\text{Te}_{0.85}$ alloys that exhibit a density anomaly between 633 K and 733 K at ambient pressure was investigated using x-ray absorption spectroscopy at the Ge K edge. Using a reverse Monte Carlo method to combine the present results with neutron scattering data, we show that the volume contraction is associated with an increase of the first neighbor coordination number around both Ge and Te by about one atom. The coordination number of Ge increases from 3 ± 0.3 to 4.1 ± 0.3 . These results support an interpretation of the density anomaly in terms of the same Peierls-like distortion mechanism acting in the liquid state and in the neighboring (pure Te and GeTe compound) phases.

DOI: [10.1103/PhysRevB.72.174209](https://doi.org/10.1103/PhysRevB.72.174209)

PACS number(s): 61.10.Ht, 61.43.Bn, 61.25.Mv, 05.10.Ln

I. INTRODUCTION

Liquid alloys of Ge and Te exhibit a series of thermodynamic anomalies in a temperature range between the eutectic temperature that is reported at 650 K¹ and 750 K and in a composition range between pure Te and about 20% Ge. The most striking features are the density anomaly² and the maxima in specific heat and isothermal compressibility^{3,4} evidenced by Tsuchiya. The same author also measured an increase of the electrical conductivity⁵ by two orders of magnitude in a 200 K range at the eutectic $\text{Ge}_{0.15}\text{Te}_{0.85}$ composition. Although the maxima of the thermodynamic response functions are rounded and of finite height, indicating that no phase transition occurs, these results show that some structural change takes place in the liquid.

Neutron or x-ray scattering experiments^{6–8} performed at the eutectic composition, where the above effects are the sharpest, agree on an essential feature: upon heating, the amplitude of the second peak of the total structure factor strongly decreases. In real space, this is related to a gradual decrease of the height of the first peak of $g(r)$ and a filling of the first minimum. An attempt to combine neutron and x-ray scattering data to calculate the partial pair correlation functions is presented in Ref. 8, but is hampered by the small q range ($q < 8 \text{ \AA}^{-1}$) of the experiments, which leads to large uncertainties in the Fourier transforms. More recently Yoshioka *et al.*⁹ performed extended x-ray absorption fine structure (EXAFS) measurements in transmission mode at

both Ge and Te K edges. They concluded that, in the 633–833 K temperature range, the partial Te—Te and Ge—Te coordination number decrease from 1.8 to 1.5 and 2.8 to 1.5 respectively, while the Te—Te and Ge—Te bond distances are increasing. Since we generally expect¹⁰ that, in a covalently bonded system, a decrease of the coordination number should go along with a decrease of the bond distances, these results seem surprising. In order to solve this apparent inconsistency we performed new EXAFS experiments at the Ge K edge and we developed a reverse Monte Carlo (RMC) method to combine these measurements with neutron scattering results.⁷ RMC modeling of experimental data was first introduced by McGreevy *et al.*^{11,12} for liquid and amorphous structures. A recent discussion of its possibilities and limitations can be found in Ref. 13. As opposed to the more general Metropolis Monte Carlo method, it does not contain any physical interatomic interaction model but it is designed to produce atomic structures that fit an experimental signal and quite often requires additional constraints to obtain physically acceptable results. It is clear that a larger set of independent experimental data should produce a better result. Combining neutron or x-ray scattering and EXAFS data is therefore a very attractive scheme. Neutron scattering experiments yield a high accuracy and a relatively easy data treatment, but are limited by the need for expensive isotopic substitutions to give an access to the partial structure factors. Combining the chemical sensitivity of EXAFS and the accuracy of the total structure factor measured by neutron scattering proves an efficient way of obtaining a quantitative

analysis of structural changes undergone by the $\text{Ge}_{0.15}\text{Te}_{0.85}$ liquid system.

II. EXPERIMENTAL DETAILS

X-ray absorption measurements were carried out at the European Synchrotron Radiation Facility (ESRF) (Grenoble, France) on the French CRG-BM30B beamline. Details on the beamline setup can be found in Ref. 14. The experiments were performed at the Ge K edge (11 103 eV) with an energy resolution of 1.6 eV. The experimental setup available at that time did not allow measuring both Ge and Te edges in the limited time allocated for the experiment. Due to the high absorption cross section of the tellurium matrix, data collection was performed in fluorescence mode using an energy resolved multielement germanium detector.

The sample was prepared by direct alloying of the pure elements (99.999% purity for Ge and Te, Alpha products). The elements were introduced as small pieces in a silica tube and sealed under vacuum. The sample was heated up to 873 K, maintained at this temperature for 10 hours to ensure the homogeneity of the melt, and then rapidly quenched to 293 K. Scanning electron microscopy coupled with an energy dispersive x-ray analysis was used to verify the formation of a eutectic mixture.

The sample was then milled and placed in powder form into the high pressure cell developed in the Laboratoire de Cristallographie (Grenoble, France). This cell, devoted to EXAFS measurements in transmission as well as in fluorescence mode, is described in detail by Testemale *et al.*¹⁵ Briefly, it consists of a polycrystalline sapphire cell which is inserted in a steel vessel. The cell contains a vertical outer sapphire tube and two alumina coaxial inner rods that delimit the sample space below and above. For the experiment reported here, we had to slightly modify the cell by replacing one inner tube by a silica capillary containing the sample. An inert gas (He) pressure was kept at 5 bars to limit the evaporation of tellurium, which is the most volatile element. We performed several heating and cooling cycles to check the reproducibility of the experiment and verified that the x-ray absorption near-edge structure (XANES) showed no sign of oxydation of the sample.

III. QUALITATIVE TRENDS IN THE EXPERIMENT

As the data were recorded in fluorescence mode, all the spectra were checked against self-absorption. This effect turned out to be negligible due to the high atomic weight of the tellurium matrix and the low germanium concentration. The analysis of the EXAFS signal was performed using the software package WINXAS v3.1¹⁶ and according to recommended procedures from the literature.¹⁷ Background subtraction and normalization was performed by fitting linear functions to the pre-edge and the postedge regions of an absorption spectrum, respectively. The measured absorption spectra $\mu(E)$ are presented in Fig. 1. The EXAFS $\chi(k)$ was obtained by using cubic splines to subtract a smooth atomic background, $\mu_0(k)$. As all the spectra were distorted beyond 11.7 keV we restricted our data analysis up to $k=10 \text{ \AA}^{-1}$.

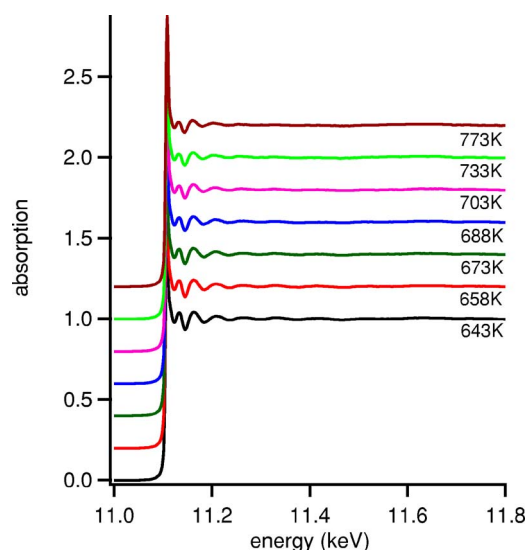


FIG. 1. (Color online) Experimental absorption $\mu(E)$ measured on the BM30B beamline between 643 K and 773 K. The curves are shifted along the y axis.

The EXAFS spectra $\chi(k)$ are presented in Fig. 2. With increasing temperature the spectra show a clear damping of the oscillations caused by the increasing thermal disorder and a phase shift towards lower wave numbers in the $4.5 < k < 8 \text{ \AA}^{-1}$ range, which are the signature of the continuous structural changes in the liquid state.

We calculated the pseudo radial distribution function $\{F(r)=FT[k^2\chi(k)]\}$ by Fourier transforming the k^2 -weighted experimental $\chi(k)$ function, multiplied by a Hanning window, into real space. The resulting Fourier transforms are plotted in Fig. 3. In agreement with the findings of Yoshioka *et al.*,⁹ we see a strong decrease of the intensity of the first peak around 2.46 \AA , which is approximately divided by 2 in the 90 K range presented.

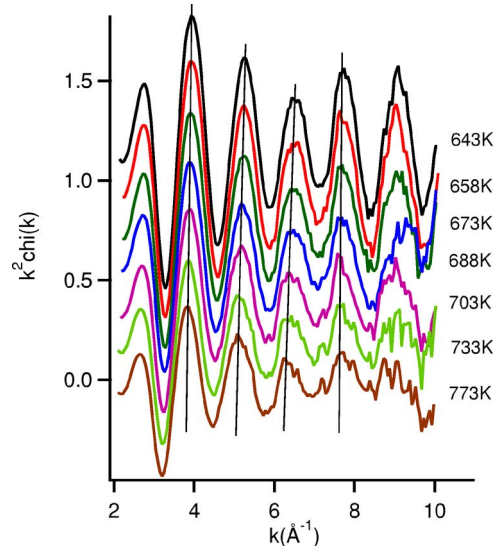


FIG. 2. (Color online) Experimental $k^2\chi(k)$ measured between 643 K and 773 K. The curves are shifted along the y axis. The thin black lines joining the maxima of the EXAFS oscillations emphasize the small k shift with increasing temperature.

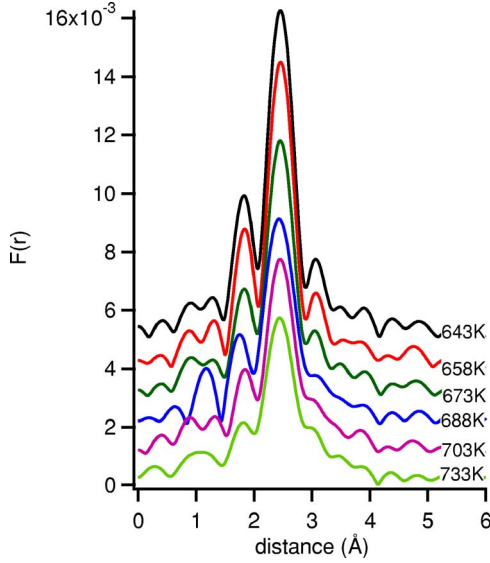


FIG. 3. (Color online) Fourier transform of the measured $k^2\chi(k)$ between 643 K and 733 K. The curves are shifted along the y axis. When the temperature is raised, the height of the peak corresponding to the first neighbor distance strongly decreases.

Pushing further, the structural analysis requires some assumptions on the shape of the peaks in the real space (Gaussians, for example, as done by Yoshioka *et al.*⁹) or, more generally, a structural model that is not available in the present case. Instead of relying on unassessed hypotheses we will show in the next sections that combining EXAFS and neutron scattering data via a RMC technique allows us to gain a significant insight into the structural changes that take place in the liquid.

IV. REVERSE MONTE CARLO METHOD

The principle of the reverse Monte Carlo method is to minimize a weighted χ^2 which, in our case, is the sum of two terms,

$$\chi^2 = \alpha \chi_{g(r)}^2 + (1 - \alpha) \chi_{\chi(k)}^2, \quad (1)$$

where

$$\chi_{g(r)}^2 = \sum_{i=1}^{N_{g(r)}} \frac{[g^{\text{exp}}(r_i) - g^{\text{calc}}(r_i)]^2}{\sigma_i^2} \quad (2)$$

for neutron data and

$$\chi_{\chi(k)}^2 = \sum_{j=1}^{N_{\chi(k)}} \frac{[\chi^{\text{exp}}(k_j) - \chi^{\text{calc}}(k_j)]^2}{\sigma_j^2} \quad (3)$$

for EXAFS data and α controls the relative weight of the two terms. $g(r)$ and $\chi(k)$ are calculated on the simulated structure at each step of the RMC procedure. σ_i and σ_j are the standard deviations estimated on $g(r)$ and $\chi(k)$ respectively. We took $\sigma_i=0.02$ and, by checking the reproducibility of different $\chi(k)$ measured at the same temperature, we estimated $\sigma_j=0.005$. It is taken constant for k between 3 and 8 \AA^{-1} and

linearly increasing outside this region. Obtaining $g(r)$ is straightforward but calculating $\chi(k)$ requires some approximations. In order to get a fast enough calculation, we use the following two-body approximation to $\chi(k)$:¹⁸

$$\chi(k) = S_0^2 R \sum_{\text{neighbors } i} \frac{F_{\text{eff}}}{kr_i^2} \exp(-2r_i/\lambda) \sin(2kr_i + \varphi), \quad (4)$$

where (i) S_0^2 is the amplitude reduction factor, (ii) R is the k -dependent reduction factor, (iii) F_{eff} is the k -dependent back scattering amplitude, (iv) λ is the k -dependent electron mean free path, (v) φ is the k -dependent phase shift, and (vi) the sum runs over neighbors at a distance r , and the wave vector is given by

$$k = \frac{\sqrt{2m(E - E_e)}}{\hbar}, \quad (5)$$

where E_e is the energy of the absorption threshold. Let us note that the structural disorder is taken into account in the RMC procedure itself so that no Debye Waller term is included. The sum in Eq. (4) runs over the neighbors. In a liquid structure they have to be defined using a cutoff distance. We chose a reasonable value, between 3.6 and 4.2 \AA , and checked that the results were stable against a variation of this parameter in this range. We start from random configurations of 700 (=100 Ge+600 Te) atoms with periodic boundary conditions at the experimental densities² (0.0277 \AA^{-3} at 633 K, 0.0282 \AA^{-3} at 673 K, and 0.02890 \AA^{-3} at 733 K). The RMC algorithm aims at minimizing the weighted χ^2 by randomly alternating atomic displacement moves and attempts to exchange the positions of Ge and Te atoms to allow for a sampling of the chemical order. The amplitude reduction factor (S_0^2), reduction factor (R), backscattering amplitude (F_{eff}), electron mean free path (λ), and phase shift (φ) are regularly updated by calling the FEFF8 code.¹⁹ In practice, as soon as the structure is close enough to the solution these quantities do not vary any longer. In order to obtain a satisfactory convergence on both $g(r)$ and $\chi(k)$ we took $\alpha=0.85$ and a real energy shift of 7.5 eV was taken to correct the threshold energy E_e in Eq. (5). Let us note that $g(r)$ describes the structure at all distances whereas $\chi(k)$ is sensitive to the local order only. We can therefore understand why the α value we took puts more weight on $g(r)$, which is more difficult to converge, than on $\chi(k)$. Typically 10^6 atomic displacements per atom and 10^3 swaps per atom were attempted to reach convergence. The only constraint we impose is to keep Ge atoms apart by adding a repulsive term to the χ^2 in Eq. (1). This assumption is reasonable in the temperature range spanned by our experiment, bearing in mind that a chemically ordered solid GeTe compound remains stable up to 1000 K.

V. REVERSE MONTE CARLO RESULTS

The resulting $g(r)$ and $\chi(k)$ are presented in Figs. 4 and 5. The temperature dependence of both $g(r)$ and $\chi(k)$ is well reproduced, although the simulated $\chi(k)$ fails at fitting the amplitude of the experimental one in the small k range

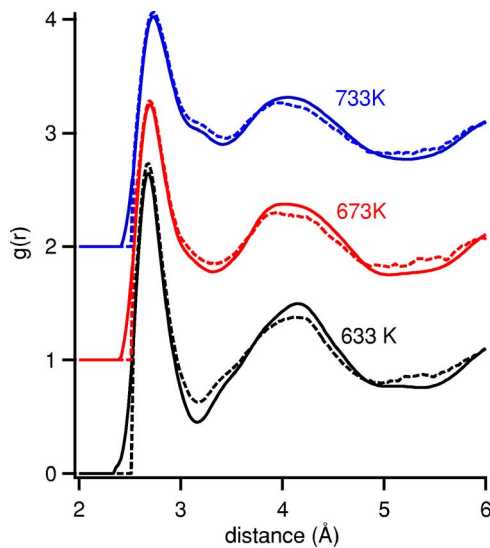


FIG. 4. (Color online) Experimental (Ref. 7) total pair correlation functions (full lines) and the corresponding result of the reverse Monte Carlo fit (dashed lines) at 633 K, 673 K, and 733 K.

($2 \text{ \AA}^{-1} < k < 6 \text{ \AA}^{-1}$). This is a consequence of the two-body approximation used in Eq. (4). In the small k range, multiple scattering contributions that are not included in the model become more important. Including n -legs loops in the EXAFS calculation using FEFF8 on the structure resulting from the RMC calculation indeed improves the agreement with the experimental $\chi(k)$ in the small k range. The gradual filling of the right-hand side part of the first peak of $g(r)$ and the outwards shift of its first minimum that is used to define the number of first neighbors in the liquid state are also well reproduced.

These features of the $g(r)$ have been interpreted as an increase in the number of first neighbors,⁷ but no quantitative analysis could be given because the neutron scattering data yield only a total structure factor. Combining neutron scat-

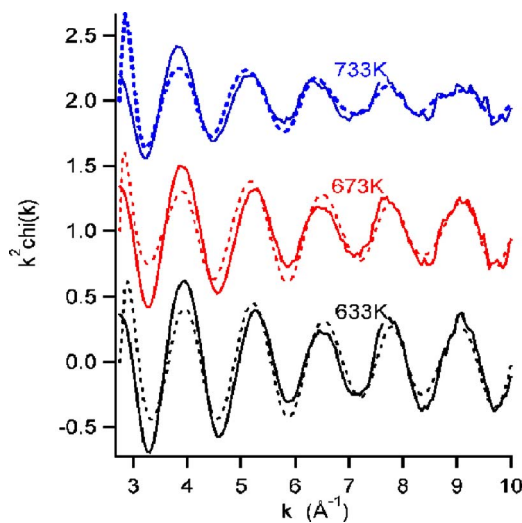


FIG. 5. (Color online) Experimental EXAFS function $k^2\chi(k)$ (full lines) and the corresponding result of the reverse Monte Carlo fit (dashed lines) at 633 K, 673 K, and 733 K.

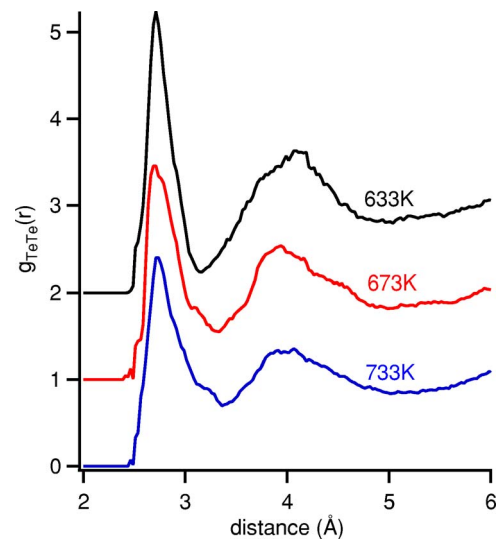


FIG. 6. (Color online) TeTe partial pair correlation functions resulting from the reverse Monte Carlo analysis at 633 K, 673 K, and 733 K.

tering and EXAFS data with the RMC analysis, we can proceed one step further by studying the partial contributions to the pair correlation function and structure factor. The $g_{TeTe}(r)$ and $g_{GeTe}(r)$ partials are presented in Figs. 6 and 7.

Because the number of Ge atoms is six times smaller than the number of Te atoms, the statistics on $g_{GeTe}(r)$ are less accurate than on $g_{TeTe}(r)$. Both partial pair correlation functions are modified by the temperature change. The right-hand side of the first peak of $g_{TeTe}(r)$ develops a shoulder with increasing temperature. It corresponds to an increase of the number of Te neighbors around each Te atom. This is qualitatively similar to what is observed in pure liquid and undercooled Te²⁰⁻²² in the same temperature range and is hardly surprising because we are dealing with a rich Te concentration ($x_{Te}=0.85$). The first neighbor shell around Ge atoms is

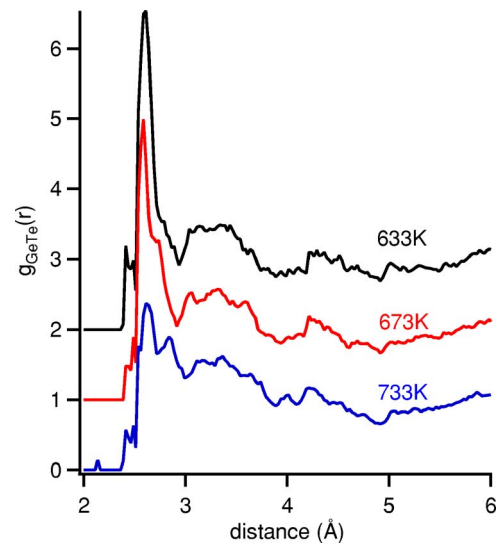


FIG. 7. (Color online) GeTe partial pair correlation functions resulting from the reverse Monte Carlo analysis at 633 K, 673 K, and 733 K.

TABLE I. Partial numbers of first neighbors calculated on the RMC generated structures.

Temperature (K)	633	673	733
Cut off distance (Å)	3.13	3.3	3.4
Number of Ge around Ge	0	0	0
Number of Te around Ge	3 ± 0.3	3.6 ± 0.3	4.1 ± 0.3
Average coordination Ge	3 ± 0.3	3.6 ± 0.3	4.1 ± 0.3
Number of Ge around Te	0.5 ± 0.1	0.6 ± 0.1	0.7 ± 0.1
Number of Te around Te	2.2 ± 0.2	2.6 ± 0.2	3.1 ± 0.2
Average coordination Te	2.7 ± 0.3	3.2 ± 0.3	3.8 ± 0.3

strongly modified. The height of the first peak at 2.61 Å decreases, a secondary peak at 2.81 Å emerges at 733 K and the overall structure is smoothed at high temperature. The decrease in height has already been noticed by Yoshioka *et al.*⁹ and interpreted as a decrease of the number of first neighbors around Ge atoms on the basis of EXAFS measurements only. Although their $\chi(k)$ and the data we present here are in excellent agreement, the calculation of the number of first neighbors by integrating up to the first minimum of the total $g(r)$ gives a different result. The result of this calculation is summarized in Table I. These values correspond to averages over 10 RMC runs under slightly different conditions and the error bars are calculated on these runs.

In the 100 K range studied that spans the density anomaly, both Ge and Te get roughly one more Te neighbor with Ge going from 3 to 4 Te neighbors and Te going from 2.7 to 3.8 neighbors. Let us remember that we have imposed a no Ge—Ge first neighbor pairs constraint. We should also keep in mind that this increase of the number of first neighbors essentially results from the outwards shift of the first minimum of $g(r)$. Taking only EXAFS data into account leads to the same results as Yoshioka *et al.*⁹ A simple fit of the $k^2\chi(k)$ indeed yields one distance (2.60 Å) at 633 K and two distances (2.61 and 2.81 Å) at 733 K but the associated numbers of neighbors are not stable and the RMC analysis provides more information. Yoshioka *et al.* nevertheless concluded to a decrease of the Ge—Te coordination number, which is hardly compatible with the increase of the Ge—Te distance noted by these authors and also seen on the Fourier transform of $\chi(k)$ presented in Fig. 3. In such covalently bonded systems, an increase of the bond distance is generally related to an increase of the coordination number. As already pointed out by Filipponi,²³ these different conclusions drawn from data that are in good agreement question the possibility of obtaining reliable structural information on a liquid structure on the basis of EXAFS experiments alone.

We can check the reliability of these RMC calculations by comparing the distribution of the bond angles of the six first neighbors around each type of atoms calculated on the RMC structures to the same quantity obtained by first principles molecular dynamics.²⁴ This comparison is displayed in Fig. 8. As expected, the RMC method yields a more disordered structure but we can see that the overall distribution is essentially correct with a tendency to favor angles in the 60–90° range, corresponding to a “hard sphere” behavior.

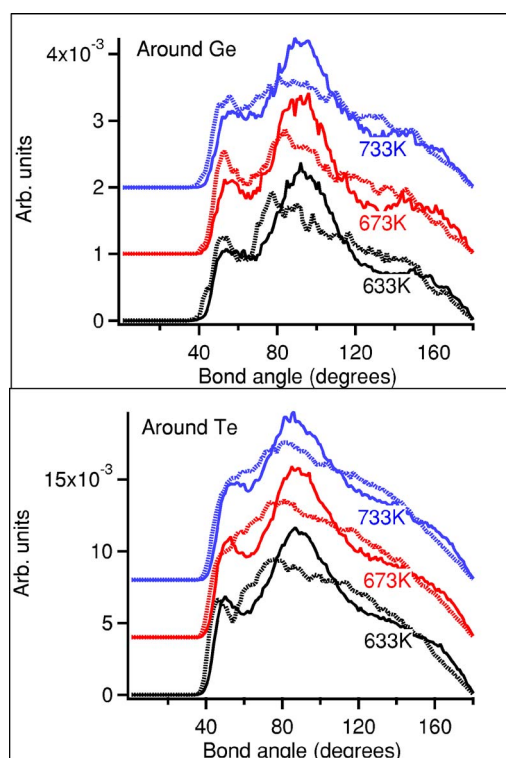


FIG. 8. (Color online) Bond angle distribution of the six first neighbors around Ge (upper panel) and Te atoms (lower panel) at 633 K, 673 K, and 733 K resulting from first principles molecular dynamics simulations (Ref. 24) (full line) and from the reverse Monte Carlo analysis (dotted lines).

Figure 9 is a plot of the RMC total structure factor compared to the experimental one. As already noted on the pair correlation functions, the local and medium range order that give significant contributions in the $q > 4 \text{ \AA}^{-1}$ range are very accurately reproduced. The strong temperature dependence of the second peak of the total structure factor is also present,

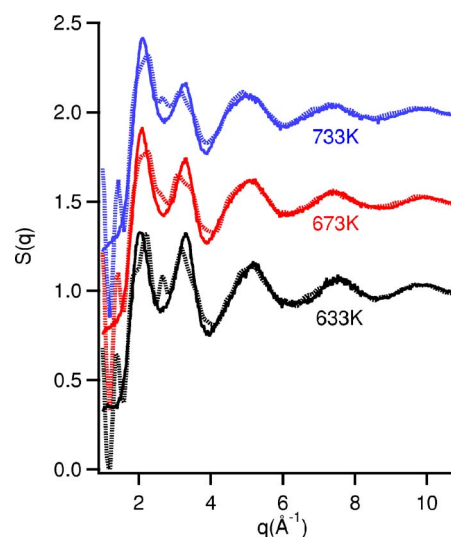


FIG. 9. (Color online) Experimental (Ref. 7) total structure factors (full lines) and the corresponding result of the reverse Monte Carlo fit (dotted lines) at 633 K, 673 K, and 733 K.

but, contrary to the *ab initio* results,²⁴ it mainly results from the $S_{TeTe}(q)$ contribution.

Within these two limitations, the RMC procedure provides a reliable insight into the structural changes undergone by liquid $Ge_{0.15}Te_{0.85}$ alloys in the temperature range of the density anomaly. The estimated change of the partial coordination numbers around Ge and Te atoms is particularly interesting since it sheds light on the possible mechanisms involved. Let us remark that integrating the number of first neighbors around Ge up to the minimum of the partial $g_{GeTe}(r)$ located around 4 Å in Fig. 6 yields a remarkably constant value between 6.5 and 7.2 neighbors at all temperatures. In the low temperature structure Ge has 3 ± 0.3 Te first neighbors at short distance (around 2.6 Å). This suggests that the same Peierls-like mechanism as that acting in the GeTe compound is responsible for the structure of the low temperature $Ge_{0.15}Te_{0.85}$ liquid phase: Ge atoms are surrounded by three Te atoms at short distances and three or four atoms at larger distances, forming an asymmetric first neighbor shell. When the temperature is raised the increase of the number of short Te neighbors leads to a more symmetric and more compact first neighbor shell, thus contributing to the volume contraction. As can be seen from the calculated $g_{GeTe}(r)$ and confirmed by a simple fit of the $k^2\chi(k)$, only one distance at 633 K and two at 733 K are sharply defined (with a small Debye Waller factor). The distances beyond are very loosely defined (with a large Debye Waller factor) and do not make significant contributions to the EXAFS signal but are observed with an equal weight on the neutron scattering data.

This is essentially the reason why combining these two sets of data is important in order to reach a physically acceptable picture of the atomic structure and its changes with temperature.

VI. CONCLUSION

In the case of a binary alloy, combining the chemical sensitivity of the EXAFS and the structural constraints imposed by the total structure factor measured by a scattering technique is an attractive scheme to obtain quantitative information on the local atomic structure. This is done by using a reverse Monte Carlo method that proves efficient in the present instance, although the only constraint that has been imposed is to keep Ge atoms apart from each other, thus assuming a chemically ordered liquid. Because there are only three first neighbors at short distance and no significant feature around 109° in the bond angle distribution, the bonding around Ge atom is not of the sp^3 type. Consequently the density anomaly studied here does not enter the classical scheme valid for tetrahedrally bonded liquids such as water.²⁵ Our results suggest that the density anomaly is related to the structural change from a liquid with a symmetry-broken local environment at low temperature stabilized by the opening of a pseudogap at the Fermi level at low temperature to a more symmetric local environment at higher temperature that has to be stabilized by the entropy gain. This scheme is confirmed by recent first principles molecular dynamics calculations.²⁴

¹A. Schlieper, Y. Feutelais, S. G. Fries, B. Legendre, and R. Blachnik, *CALPHAD: Comput. Coupling Phase Diagrams Thermochem.* **23**(1), 1 (1999).

²Y. Tsuchiya, *J. Phys. Soc. Jpn.* **60**, 227 (1991).

³R. Castanet and C. Bergman, *Phys. Chem. Liq.* **14**, 219 (1985).

⁴Y. Tsuchiya, *J. Non-Cryst. Solids* **156–158**, 704 (1993).

⁵Y. Tsuchiya and H. Saitoh, *J. Phys. Soc. Jpn.* **62**, 1272 (1993).

⁶E. Nicotera, M. Corchia, G. De Giorgi, F. Villa, and M. Antonini, *J. Non-Cryst. Solids* **11**, 417 (1973).

⁷C. Bergman, C. Bichara, J.-P. Gaspard, and Y. Tsuchiya, *Phys. Rev. B* **67**, 104202 (2003).

⁸H. Neumann, W. Matz, W. Hoyer, and M. Wobst, *Phys. Status Solidi A* **90**, 489 (1985).

⁹S. Yoshioka, Y. Kawakita, M. Kanehira, and S. Takeda, *Jpn. J. Appl. Phys., Part 1* **38**, 468 (1999).

¹⁰J.-P. Gaspard, A. Pellegatti, F. Marinelli, and C. Bichara, *Philos. Mag. B* **77**, 727 (1998).

¹¹S. J. Gurman and R. L. McGreevy, *J. Phys.: Condens. Matter* **2**, 9463 (1990).

¹²R. L. McGreevy and L. Pusztai, *Mol. Simul.* **1**, 359 (1988).

¹³R. L. McGreevy, *J. Phys.: Condens. Matter* **13**, R877 (2001).

¹⁴O. Proux, X. Biquard, E. Lahera, J. J. Menthonnex, A. Prat,

O. Ulrich, Y. Soldo, P. Trivison, G. Kapoujyan, G. Perroux, P. Taunier, D. Grand, P. Jeantet, M. Deleglise, J. P. Roux, and J. L. Hazemann, *Phys. Scr., T* **T115**, 970 (2005).

¹⁵D. Testemale, R. Argoud, O. Geaymond, and J.-L. Hazemann, *Rev. Sci. Instrum.* **76**, 43905-1 (2005).

¹⁶T. Ressler, *J. Synchrotron Radiat.* **5**, 118 (1998).

¹⁷D. C. Koningsberger and R. Prins, *X-Ray Absorption Spectroscopy, Chemical Analysis* (Wiley, New York, 1988), Vol. 92.

¹⁸J. Als-Nielsen and D. McMorrow, *Elements of Modern X-Ray Physics* (J. Wiley, New York, 2001).

¹⁹A. L. Ankudinov, B. Ravel, J. J. Rehr, and S. D. Conradson, *Phys. Rev. B* **58**, 7565 (1998).

²⁰A. Menelle, R. Bellissent, and A. M. Flank, *Europhys. Lett.* **4**, 705 (1987).

²¹C. Bichara, J.-Y. Raty, and J. P. Gaspard, *Phys. Rev. B* **53**, 206 (1996).

²²S. de Panfilis and A. Filipponi, *Europhys. Lett.* **37**, 397 (1997).

²³A. Filipponi, *J. Phys.: Condens. Matter* **13**, R23 (2001).

²⁴C. Bichara, M. Johnson, and J.-Y. Raty, *Phys. Rev. Lett.* (to be published).

²⁵P. G. Debenedetti, *J. Phys.: Condens. Matter* **15**, R1669 (2003).